Chemical composition dependent Raman scattering spectroscopy of MBE grown magnesium- based bismuth telluride topological insulator thin films

N. Kumar*[1,2], D.V. Ishchenko[1], I.A. Milekhin[1,3], E.D. Kyrova[1,4], A. G. Milekhin[1,3], O.E. Tereshchenko[1,5,6]

[1]Rzhanov Institute of Semiconductor Physics, SB RAS, Novosibirsk, 630090, Russia.

[2]Tomsk State University, 36 Lenin Ave., Tomsk, 634050 Russia.

[3]Novosibirsk State University, Novosibirsk, 630090, Russia.

[4]Novosibirsk State Technical University, Novosibirsk, 630073, Russia.

[5]Synchrotron Radiation Facility SKIF, Boreskov Institute of Catalysis, SB, RAS, Koltsovo 630559, Russia.

[6]Department of Physics, Saint Petersburg State University, St. Petersburg 198504, Russia.

Abstract

Chemical composition dependent vibrational modes of MBE grown magnesium-based bismuth telluride (MBT) magnetic topological insulators thin films were studied by Raman spectroscopy and compared with the vibrational modes of Bi_2Te_3 films. Intensity of E_g^3 TO mode was much stronger in Bi reach MBT film. In contrast, intensity of A_{1g}^2 LO mode was stronger in Bi deficient MBT compound. E_g^3 TO mode corresponds to in-plane vibrations of the top and the bottom Bi-Te atomic layers in the manner similar to that of Bi_2Te_3. Deficiency of Bi atoms in the MBT indicated that the vibrational degree of freedom of Bi-Ti in the septuple unit cell was less probable. Antisymmetric out-of-phase vibration of Te-Te atoms resulted in A_{1g}^2 LO mode in which Bi atom was stationary, therefore vibrational cross section of this mode for Bi deficient MBT film was stronger. Near resonance condition of E_g and A_{1g} modes was observed at lower excitation energy 1.57 eV associated to deformation potential and Frohlich electron-phonon coupling, respectively.

Keywords: Magnetic topological insulators, polarization-resolved resonant Raman spectroscopy, vibrational modes.

*E-mail: kumar@isp.nsc.ru

1. Introduction

Three-dimensional topological insulators (3DTIs) obey the time reversal symmetry originating from spin-orbit interaction, which consists of an insulating bulk and a gapless surface state where dispersion of electron is linear [1–5]. However, magnetism breaks the time reversal symmetry leading to gap opening in the surface of topological states due to magnetic exchange interaction [6–8]. This can lead to numerous novel topological quantum states including quantum anomalous Hall effect, axion insulator and magnetic Weyl semimetallic phase [6–8].

Manganese-based bismuth telluride (MBT) is a widely studied magnetic topological insulator materials [11]. This consists of Te-Bi-Te-Mn-Te-Bi-Te septuple layers (SLs) stacking in the ABC sequence along the c-axis. Therefore, it can be viewed as a Bi_2Te_3 topological insulator by inserting a Mn-Te layer into the middle of Te-Bi-Te-Bi-Te quintuple layer (QL). According to Hund's rule each Mn^{2+} in high-spin configuration adds 5 μB magnetic moment. The intralayer exchange coupling between Mn atoms exhibits ferromagnetic order along an out-of-plane easy axis, while the interlayer exchange coupling between neighboring SLs is antiferromagnetic (AFM), generating a three-dimensional A-type antiferromagnetic order [9–11].

Many compelling properties of magnetic topological materials originate from the gapped electron surface states that are protected by discrete symmetry. A scattering between charge carriers and lattice vibrations is one of the elementary interactions in condensed matter system which manifest to modify the various physical properties. The microscopic understanding of this process is vital for the analysis of a wide range of phenomena including transport of charge carriers [12, 13]. At finite temperature, electron−phonon interaction is believed to be the main scattering mechanism of surface states [13]. In this regard investigation of lattice dynamics and phonon modes of MBT is a relevant task to study. Raman scattering is an important non-destructive method for probing the lattice dynamics and vibrational modes. Recently, Raman

spectroscopy was used to explore the lattice dynamics and resultant vibrational modes of $MnBi_2Te_4$ [14, 15]. Raman modes in $MnBi_{2n}Te_{3n+1}$(n = 1, 2, 3, 4) magnetic topological heterostructures was studied by Cho et al [16]. The vibrational modes in Raman spectroscopy with the variation of their composition in MBT is so far not clearly understood.

Here, we proposed to study chemical composition dependent vibrational modes of MBE grown MBT topological insulator thin films with the comparison of the modes of Bi_2Te_3 using polarization-resolved Raman spectroscopy at various excitation energy of photons (E_p).

2. Experimental

MBE method was used for the growth of Bi_2Te_3 and MBT topological insulators thin films on the Si (111) substrate with the variation of chemical composition. Chemical composition of the MBT compounds was investigated by X-ray photoelectron spectroscopy and the sets of samples are presented in table 1. It is worth mentioning that first three samples can be considered as Bi deficient films (1-3) and three last are Bi efficient films (4-6).

Table 1. Chemical composition and film thickness of magnetic topological insulator grown by MBE method.

No.	Chemical composition	Film thickness (nm)
1	Mn_2BiTe_4	45
2	$MnBiTe_2$	25
3	$Mn_{1.3}BiMnTe_{2.5}$	20
4	$MnBi_{1.7}Te_{2.8}$	40
5	$MnBi_{2.2}Te_{3.5}$	45
6	$MnBi_2Te_{2.8}$	35

A micro-Raman spectrometer with backscattering configuration was performed for the investigation of phonon modes in these materials. Polarization-resolved Raman spectroscopy in polarization directions V−V, H−H and V−H configuration was used. In the case of V−V and H−H polarization, both the A_{1g} and E_g tensors can be measured, whereas in the V−H

polarization geometry only a mode of E_g symmetry is allowed. In order to obtain the resonance condition, lasers of various photon energies, $E_p = 1.57$, 1.94 and 2.3 were used for the lattice and resonant electronic excitation. All spectra were obtained at room temperature and ambient pressure with the 1800 lines/mm grating and spectral resolution 1-2 cm^{-1}. Raman line width represent broadening caused by the spectrometer and the Lorentz oscillatory distribution of phonons in the crystal lattice. It is usually assumed that the spectrometer enforces a Gaussian characteristic from the crystal lattice, which itself is Lorentzian in nature. Thus, Raman spectra data were selected using mathematical convolution of these functions using the Voigt profile [17].

3. Results and discussion

Raman spectra of MBT is similar to Bi_2Te_3 [14, 15], because of similarity in the symmetry of crystal structure. The crystal structure of Bi_2Te_3 and MBT consists of five (Te-Bi-Te-Bi-Te) and seven atomic layers (Te−Bi−Te−Mn−Te−Bi−Te) stacked along the *c*-direction, respectively. Bi_2Te_3 consist of four Raman active modes, two of them is transverse optical (TO) mode of E_g symmetry (E_g^1 and E_g^2) and other two are longitudinal optical (LO) mode of A_{1g} symmetry (A_{1g}^1 and A_{1g}^2). E_g and A_{1g} describes shear mode with in-plane and breathing mode due to out-of-plane atomic displacements, respectively. According to group theory, $MnBi_2Te_4$ contains doubly degenerate E_g and nondegenerate A_{1g} symmetry Raman modes [16]. It must have six Raman active modes: $3E_g$ (E_g^1, E_g^2 and E_g^3), and $3Ag$ (A_{1g}^1, A_{1g}^2 and A_{1g}^3) modes. The vibrational modes of Bi_2Te_3 and MBT are shown in schematic diagram (Fig. 1), this will be further discussed below.
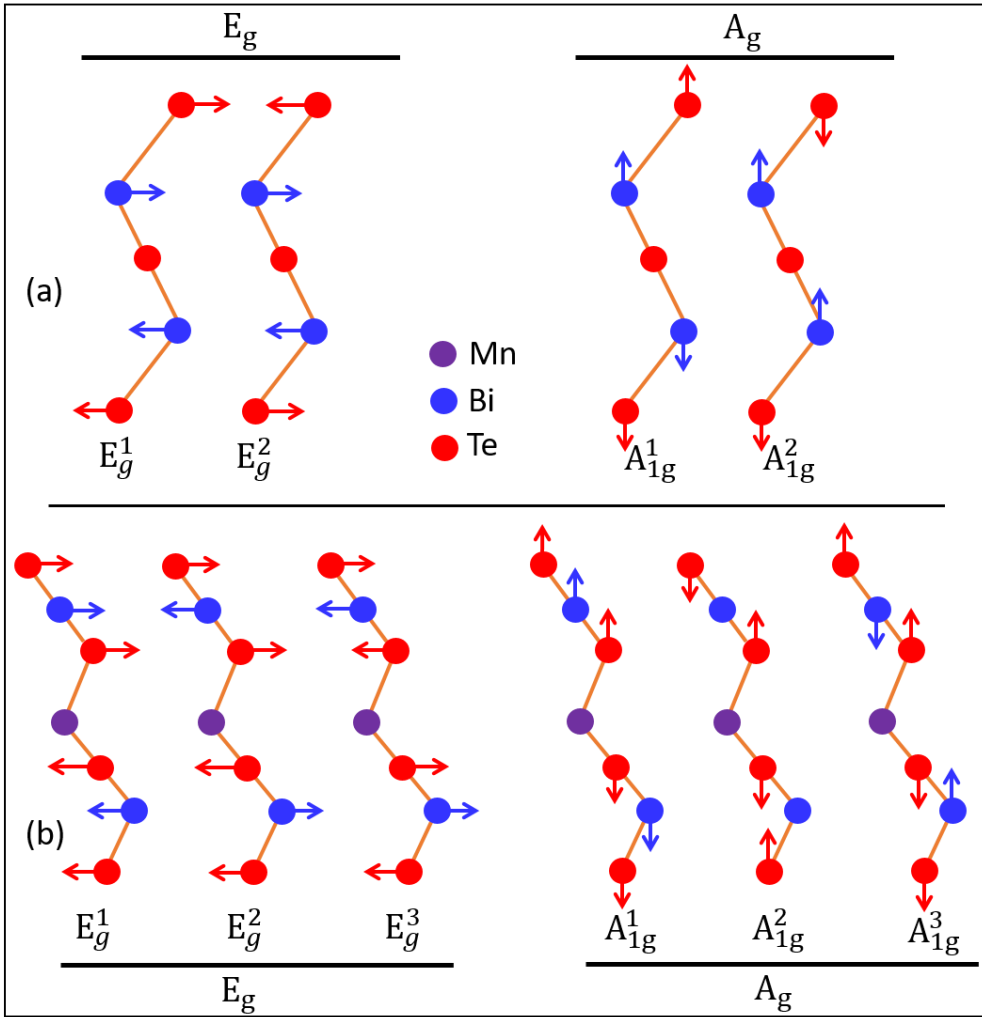
Fig. 1. Raman active vibrational degree of freedom of (a) Bi_2Te_3 and (b) MBT chains; 4 and 6 degree of freedom of vibrations in Bi_2Te_3 and MBT, respectively.

Chemical composition dependent Raman spectroscopy of MBT films are shown in Fig. 2 at three different E_p 2.33, 1.94 and 1.57 eV with linearly polarized light. The results can be mainly divided into two distinct parts, in one part the intensity of A_{1g}^2 mode is strong at all the three E_p (films 1 to 3 in table 1). In other parts, the intensity of E_g^2 mode is stronger at all the three E_p (films 4 to 6 in table 1). It can be seen that E_g^2 mode is stronger in intensity when Bi atom is efficient in the compound. However, Bi deficient compound showed stronger intensity of A_{1g}^2 mode. It can be argued that the potential energy of the oscillator and phonon density of states mainly depend upon the number of Bi atoms in the unit cell.
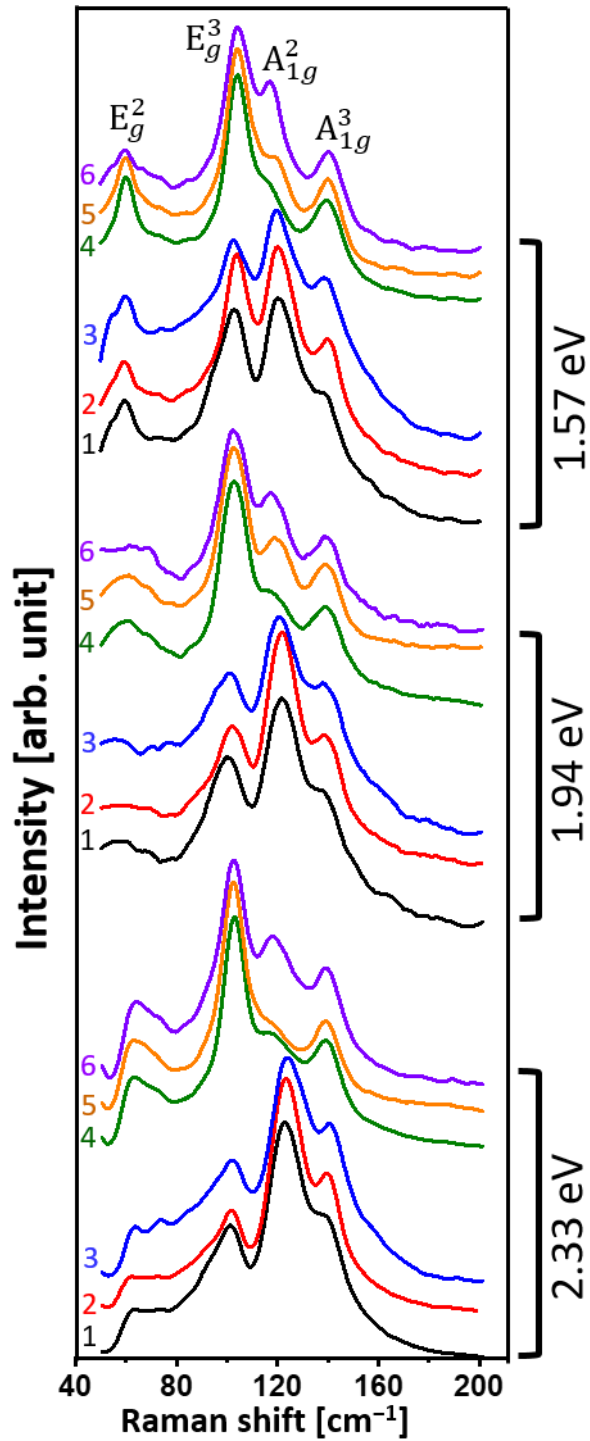
Fig. 2. Chemical composition dependent Raman spectroscopy of magnetic topological insulators: 1 – Mn_2BiTe_4, 2 – $MnBiTe_2$, 3 – $Mn_{1.3}BiMnTe_{2.5}$, 4 – $MnBi_{1.7}Te_{2.8}$, 5 – $MnBi_{2.2}Te_{3.5}$ and 6 – $MnBi_2Te_{2.8}$ at three different excitation energy of photons 2.33, 1.94 and 1.57 eV.

Other differences in the spectra includes resonant excitation of E_g^2 mode at E_p 1.57 eV for all the films, however, this mode is weak at E_p 2.33 eV. The intensity of A_{1g}^2 mode is sensitive to Bi atoms, intensity of this mode increases for higher contribution of Bi atoms in the compound (films 5 and 6) at all the E_p. However, intensity of A_{1g}^3 mode is not sensitive to Bi atoms in the films 4 to 6, and the intensity of this mode is almost similar for all the E_p. Due to lattice expansion a redshift of Raman modes of A_{1g}^2 was observed at lower excitation energy of Bi deficient film. Low frequency shifts of this mode in Bi efficient sample compared to Bi deficient in all the E_p can be explained by oscillator strength, considering mass and spring constant of the oscillator. In Bi efficient sample the displacement of Bi-Te atoms, and in Bi deficient sample displacement of Te-Te atoms in the oscillator is considered.

From the above results one can select any two distinct samples out of six, for example: Bi deficient $Mn_{1.3}BiTe_{2.5}$ (sample number 3) and Bi efficient $MnBi_{1.7}Te_{2.8}$ MBT films (sample number 4) for detail study, and comparing the results with Bi_2Te_3 film. Raman spectroscopy of these samples at excitation energy E_p 1.57, 1.94 and 2.3 eV with linearly polarized light are shown in Fig. 3. Corresponding surface topography of these films are also resented in this figure. Bi_2Te_3 film showed steps-like feature which indicates layered structure, in MBT such distinct layer is absent because for misoriented planes and defects.

At first, we present the results of Bi_2Te_3 in curves (a), (b) and (c) which showed three distinct and strong Raman peaks $2A_{1g}$ (A_{1g}^1, and A_{1g}^2) and $1E_g$ (E_g^2) modes indicated by peaks 1, 2 and 3, respectively (Fig. 3). We have not observed low frequency E_g^1 vibrational mode because of low frequency cutoff of spectrometer. The intensity of E_g^2 mode is stronger in Bi_2Te_3 film in off resonance condition for E_p 1.94 and 2.3 eV which must be driven by deformation potential.
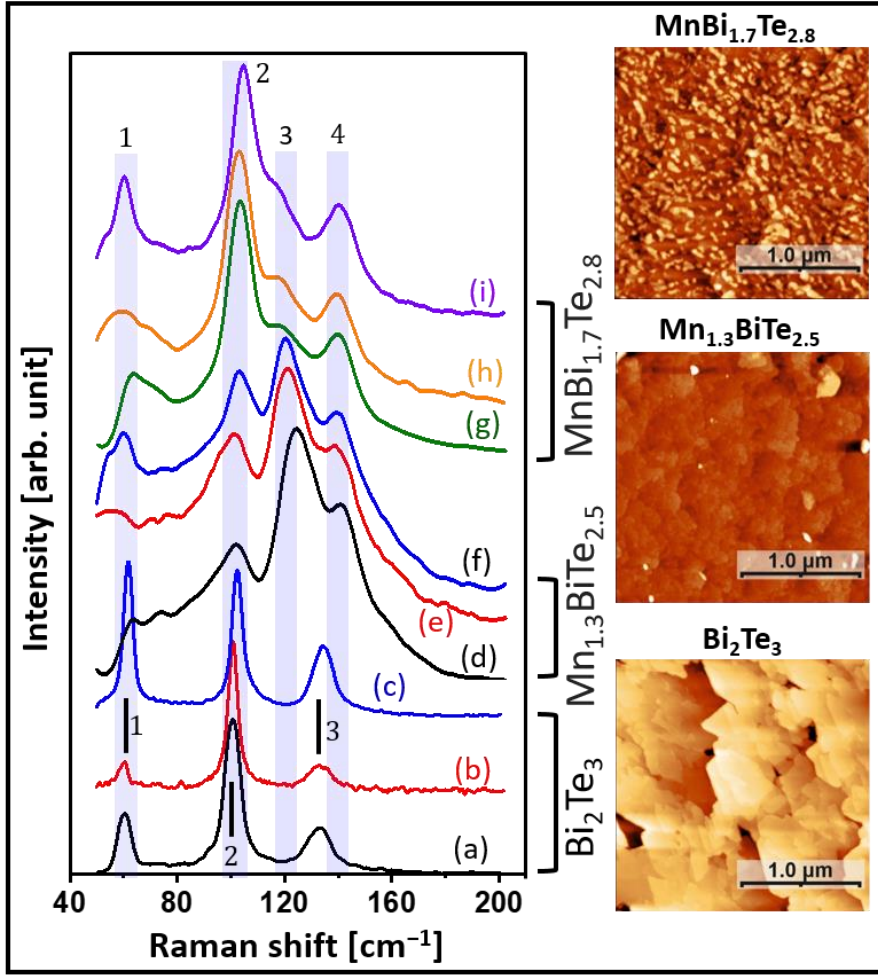
Fig. 3. Raman spectra of Bi_2Te_3 (a-c), $Mn_{1.3}BiTe_{2.5}$ (d-f) and $MnBi_{1.7}Te_{2.8}$ (g-i) with excitation energy 2.3 eV curves (a), (d), (g); 1.94 eV curves (b), (e), (h); 1.57 eV curves (c), (f), and (i), and corresponding AFM images.

This potential is based on the deformation of the atomic lattice by phonons, leading to the indirect interaction with an electron via the modulations of the periodic potential of lattice [18]. Intensity of A_{1g}^1 LO mode is higher compared to E_g^2 mode at E_p 1.57 eV which satisfies the resonance condition between electronic transition of first occupied and second unoccupied Dirac states [19−21]. At higher E_p 2.3 eV, the intensity of this mode (A_{1g}^1 LO) is slightly lower compared to E_p 1.57 eV. However, intensity of this mode is much weaker at E_p 1.94 eV which is off resonance condition [19−21]. At E_p 2.3 eV, near resonance condition is manifested due to electronic transition between the Dirac state and higher order bulk conduction band

[19−21]. The probability of this resonance is weak because of asymmetric crystal momentum of Dirac and bulk conduction band. Therefore, the intensity of A_{1g}^1 LO mode is weaker in case of E_p 2.3 eV compared to 1.57 eV. The dominance of A_{1g}^1 LO mode in resonance excitation of 1.57 eV can be explained by coupling of phonons to the electronic states, which is mediated via Frohlich electron-phonon interaction [18, 22, 23]. It is worth mentioning that only LO mode satisfies Frohlich electron-phonon interaction. It involves the direct coupling of the polarization of the lattice vibrations to the electronic charge in the following manner.

$$\mathbf{P(r)} = \frac{\hbar\Omega_{LO}\epsilon_0}{e}\sum_{\mathbf{p}} g_{\mathbf{p}}^{\gamma}\frac{\mathbf{p}}{|\mathbf{p}|}e^{i\mathbf{p.r}}\left(d_{\mathbf{p}} - d_{-\mathbf{p}}^{\dagger}\right) \tag{1}$$

where, $\frac{\mathbf{p}}{|\mathbf{p}|}\left(d_{\mathbf{p}} - d_{-\mathbf{p}}^{\dagger}\right)$ describes the quantized version of induced displacement with Boson creation and annihilation operators $d_{-\mathbf{p}}^{\dagger}$ and $d_{\mathbf{p}}$ for phonon with wave vector $\mathbf{p}$, $\hbar\Omega_{LO}$ is LO phonon energy, ϵ_0 is vacuum permittivity, and $g_{\mathbf{p}}^{\gamma}$ is Frohlich matrix element. The associated polarization creates a macroscopic field via a Coulombic term, and the band-independent Frohlich matrix element can be written as follows:

$$\left|g_{\mathbf{p}}^{\gamma}\right|^2 = \frac{e^2}{\epsilon_0\xi^3 2\hbar\Omega_{LO}}\frac{1}{|\mathbf{p}|^2}\left[\frac{1}{\epsilon(\infty)} - \frac{1}{\epsilon(0)}\right]; \gamma = \{CB, VB\} \tag{2}$$

where, ξ^3 is normalized volume of unit cell, CB and VB is conduction and valence bands, respectively, $\epsilon(\infty)$ and $\epsilon(0)$ is dielectric constants for both high-frequency and low-frequency, respectively, into Frohlich matrix element $g_{\mathbf{p}}^{\gamma}$. The momentum exchange between the electron and LO phonon is described as $\mathbf{p}$. The lattice vibrations couple with γ electrons with momentum $\mathbf{k}$, which is described by the phonon-carrier interaction, and in this case the Hamiltonian takes the following form [23]:

$$H_{ph} = \hbar\Omega_{LO} \sum_{\gamma,\mathbf{k},\mathbf{p}} g_{\mathbf{p}}^{\gamma} a_{\gamma,\mathbf{k-p}}^{\dagger} a_{\gamma,\mathbf{k}}\left(d_{-\mathbf{p}} - d_{\mathbf{p}}^{\dagger}\right) \tag{3}$$

where, $a_{\gamma}^{\dagger}$ and a_{γ} is Fermion creation and annihilation operators.

On the other hand, deformation-potential coupling originates from the variations of the bond lengths and bond angles that locally change the electronic band energies and lead to strongly band dependent matrix elements. The resulting carrier-phonon interaction has the same form as described in equation (2); however, one needs to replace $g_{\mathbf{p}}^{\gamma}$ by the deformation potential matrix element $g^{\gamma,\text{def}}$ which is described by reduced mass, deformation potential constant d^{γ} and lattice parameter a [18, 23]:

$$\left|g^{\gamma,\text{def}}\right|^2 = \frac{1}{2\rho\xi^3\Omega_{TO+LO}^3} \frac{(M_1+M_2)}{2M_1M_2} \frac{|d^{\gamma}|^2}{a^2} \tag{4}$$

where ρ is the density of the material, M_1 and M_2 are the masses of the two basis atoms in the unit cell. From the above relationship, it can be seen that the Frohlich matrix element $g_{\mathbf{p}}^{\gamma}$ depend upon the inverse of $\hbar\Omega_{LO}$, dielectric constants, and inverse mode square of wave vector $\frac{1}{|\mathbf{p}|^2}$. It means that the Frohlich coupling is strong for phonon with lower wave vector $\mathbf{p}$. However, matrix element of deformation potential $g^{\gamma,\text{def}}$ weakly depend upon energy of LO and TO phonon as $\frac{1}{\Omega_{(TO+LO)}^3}$.

Matrix element showed that Frohlich interaction decays for large $\mathbf{k}$ and it is, therefore, efficient for exchanging small momenta between electrons and phonons in resonance condition at $\mathbf{k}=0$ which showed resonantly excited peak of A_{1g}^1 LO mode in Bi_2Te_3 at E_p 1.57 eV. In deformation potential, carrier-phonon scattering mechanism is based on the

deformation of the atomic lattice by a phonon. The strength of the deformation potential scattering is essentially constant in **k** and leads to a relatively weak dependence of the coupling on the transferred momentum. Nevertheless, for small **k** values, the absolute interaction strength is considerably smaller compared to the Frohlich interaction [18]. A deformation potential is caused by both the LO and TO phonon interaction with lattices, however, Frohlich coupling is mediated by LO phonon.

In $Mn_{1.3}BiTe_{2.5}$ (curves d-f) and $MnBi_{1.7}Te_{2.8}$ (curves g-i) films, out of six, we have observed four distinct strong Raman active modes: two of E_g modes (E_{1g}^2 – peak 1 and E_g^3 – peak 2), and two of A_{1g} modes (A_{1g}^2 – peak 3 and A_{1g}^3 – peak 4) shown in Fig. 3. Other two low frequency E_{1g}^1

Depending upon the chemical composition of $Mn_{1.3}BiTe_{2.5}$ and $MnBi_{1.7}Te_{2.8}$, peak intensity of E_g^2, A_{1g}^2 and A_{1g}^3 distinctly differs as shown in deconvoluted spectra Fig. 4.
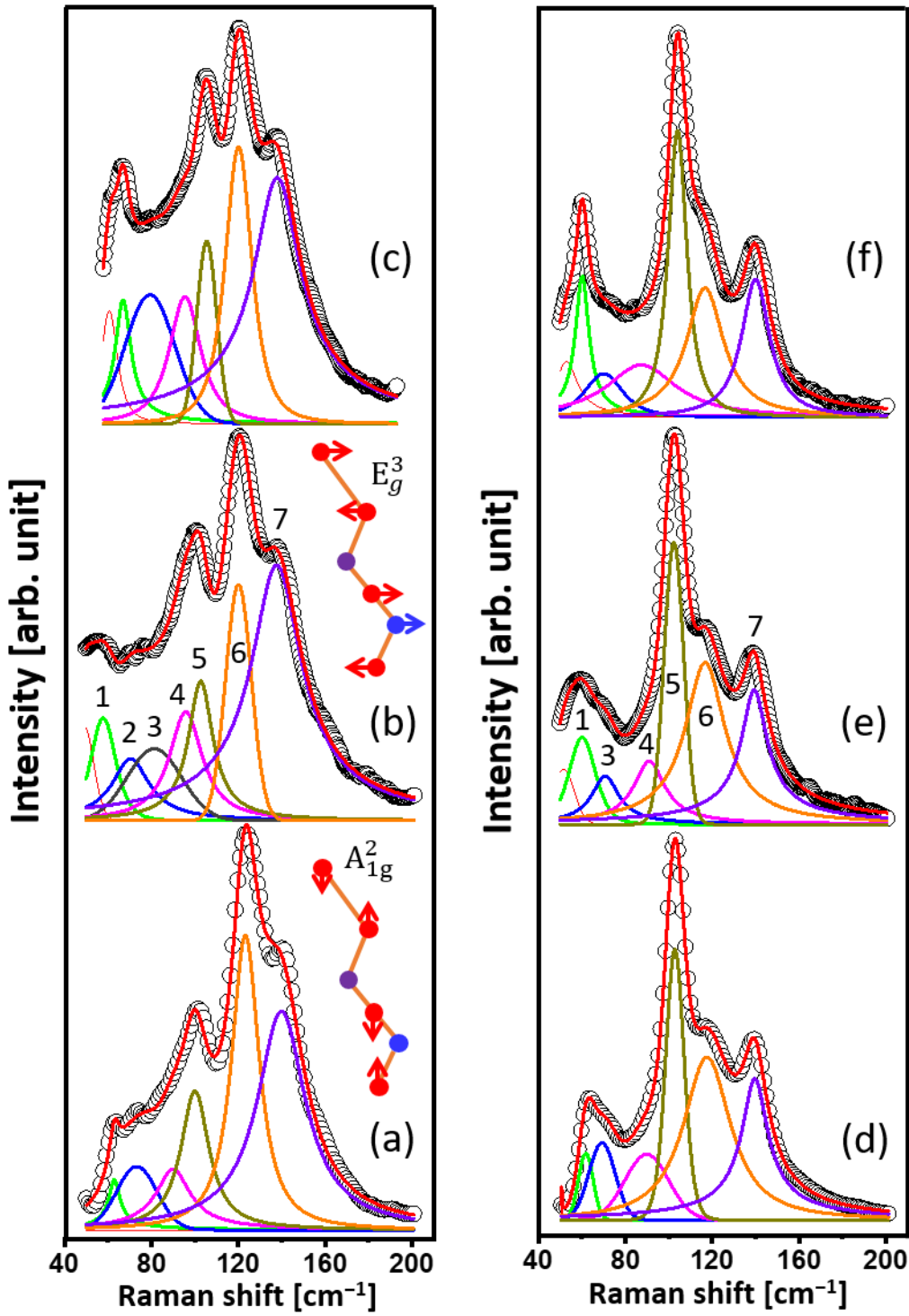
Fig. 4. Raman spectra of $Mn_{1.3}BiTe_{2.5}$ (a-c), and $MnBi_{1.7}Te_{2.8}$ (d-f); excitation energies of 2.3 eV curves (a) and (d), 1.94 eV curves (b) and (e), and 1.57 eV curves (c) and (f); peaks 1, 5, 6 and 7 – E_g^2, E_g^3, A_{1g}^2 and A_{1g}^3 modes, respectively.

The intensity of E_g^3 mode is much stronger in $MnBi_{1.7}Te_{2.8}$ compared to $Mn_{1.3}BiTe_{2.5}$ sample. However, intensity of A_{1g}^2 mode is stronger in $Mn_{1.3}BiTe_{2.5}$ sample. Peaks 1, 5, 6, and 7

belongs to Raman active modes [24−26], others are Raman forbidden IR-active modes [24−27]. Peak 5 is E_g^3 mode which is much stronger in $MnBi_{1.7}Te_{2.8}$ sample. However, peak 6 belongs to A_{1g}^2 symmetry and it is stronger in $Mn_{1.3}BiTe_{2.5}$ sample. The ratio of peak intensity of E_g^3/A_{1g}^2 and E_g^3/A_{1g}^3 can be considered as more effective way to describe the intensity variation of these modes as shown in Fig. 5.
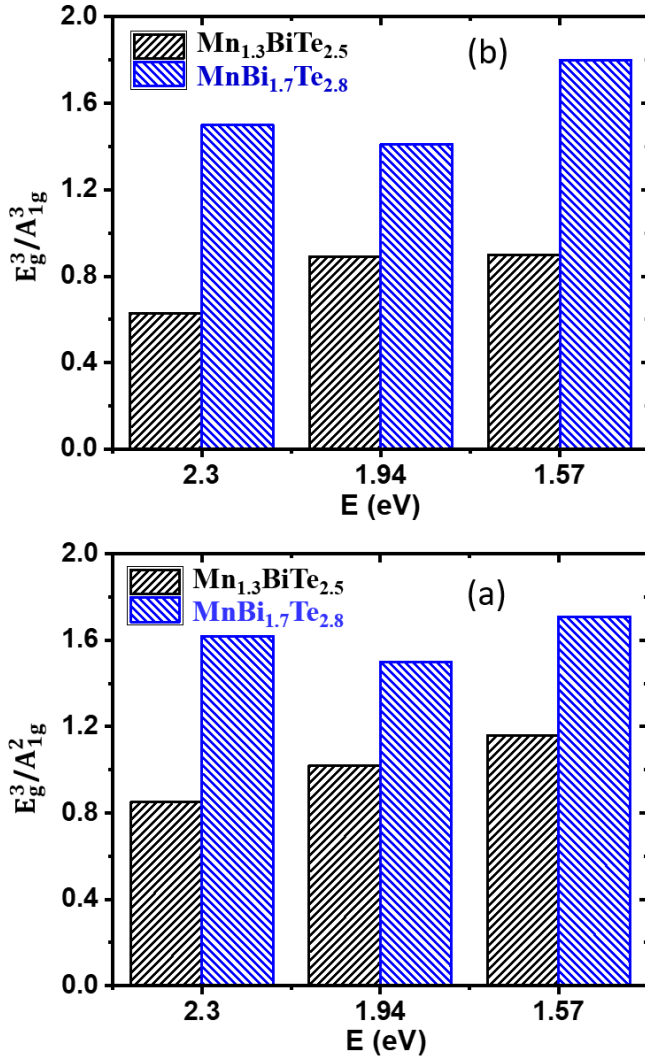
Fig. 5. Excitation energy dependent intensity ratio of E_g^3/A_{1g}^2 and E_g^3/A_{1g}^3 modes in $Mn_{1.3}BiTe_{2.5}$ and $MnBi_{1.7}Te_{2.8}$ samples.

It can be shown that the ratio of E_g^3/A_{1g}^2 and E_g^3/A_{1g}^3 is much lower in $Mn_{1.3}BiTe_{2.5}$ sample. With decrease in E_p, the ratio of E_g^3/A_{1g}^2 and E_g^3/A_{1g}^3 increases for $Mn_{1.3}BiTe_{2.5}$ which indicate that the deformation potential [18, 28] of TO mode in the matrix element is more favorable at

lower E_p 1.57 eV. However, for MnBi$_{1.7}$Te$_{2.8}$ film, the ratio of E_g^3/A_{1g}^2 and E_g^3/A_{1g}^3 is lower for E_p 1.94 eV and highest for E_p 1.57 eV.

The main contribution to the E_g^3 mode comes from the vibrations of the top and the bottom Bi-Te atomic layers, similar to that of Bi$_2$Te$_3$. In the case of Mn$_{1.3}$BiTe$_{2.5}$, the Bi atom is deficient in the chain, it means the phonon vibrational cross section of this mode is lower. The deficiency of atom in the chain is shown in the inset of Fig. 4. However, the symmetry of the septuple layer of chain in the case of MnBi$_{1.7}$Te$_{2.8}$ is preserved which causes vibrations of the top and the bottom Bi-Te atomic layers in phase, hence higher vibrational cross-section of E_g^3 mode.

The intensity of A_{1g}^2 mode is stronger in Mn$_{1.3}$BiTe$_{2.5}$ compared to MnBi$_{1.7}$Te$_{2.8}$. In A_{1g}^2 mode, the Bi atom is stationary and it does not displaces from their center of mass position. The displacement of Te-Te atoms is not disrupted in case if Bi atom in the chain of unit cell is deficient. In fact, the vibrational cross section of Te-Te atoms is more efficient which showed higher intensity of peak in Mn$_{1.3}$BiTe$_{2.5}$ film. In both type of vibrations, either Bi-Te or Te-Te in the unit cell, the frequency of A_{1g}^2 mode is different because the difference in reduced mass and oscillator strength of Bi-Te or Te-Te. Intensity of A_{1g}^2 in Mn$_{1.3}$BiTe$_{2.5}$ is weak compared to MnBi$_{1.7}$Te$_{2.8}$ because in this mode three atoms top and three atoms bottom with the combination of Bi-Te displaces in out-of-phase in antisymmetric direction. From the results one can notice that the intensity of E_g^2 and E_g^3 mode increases with decreasing the E_p which may be related with enhancement of deformation potential. The peak width of all the modes is much narrow for Bi$_2$Te$_3$ film compared to MBT which directly correspond to long range ordering of crystal structure in Bi$_2$Te$_3$ film.

Polarization induced Raman spectra of Bi$_2$Te$_3$ and MnBi$_{1.7}$Te$_{2.8}$ films are shown in Fig. 6 in H−H, V−V and V−H scattering configurations. Both H−H and V−V probe the diagonal elements $z(x, x)\bar{z}$ in Porto notation, and V−H probe the off-diagonal $z(x, y)\bar{z}$ elements of the Raman tensor [22, 23, 27, 28].
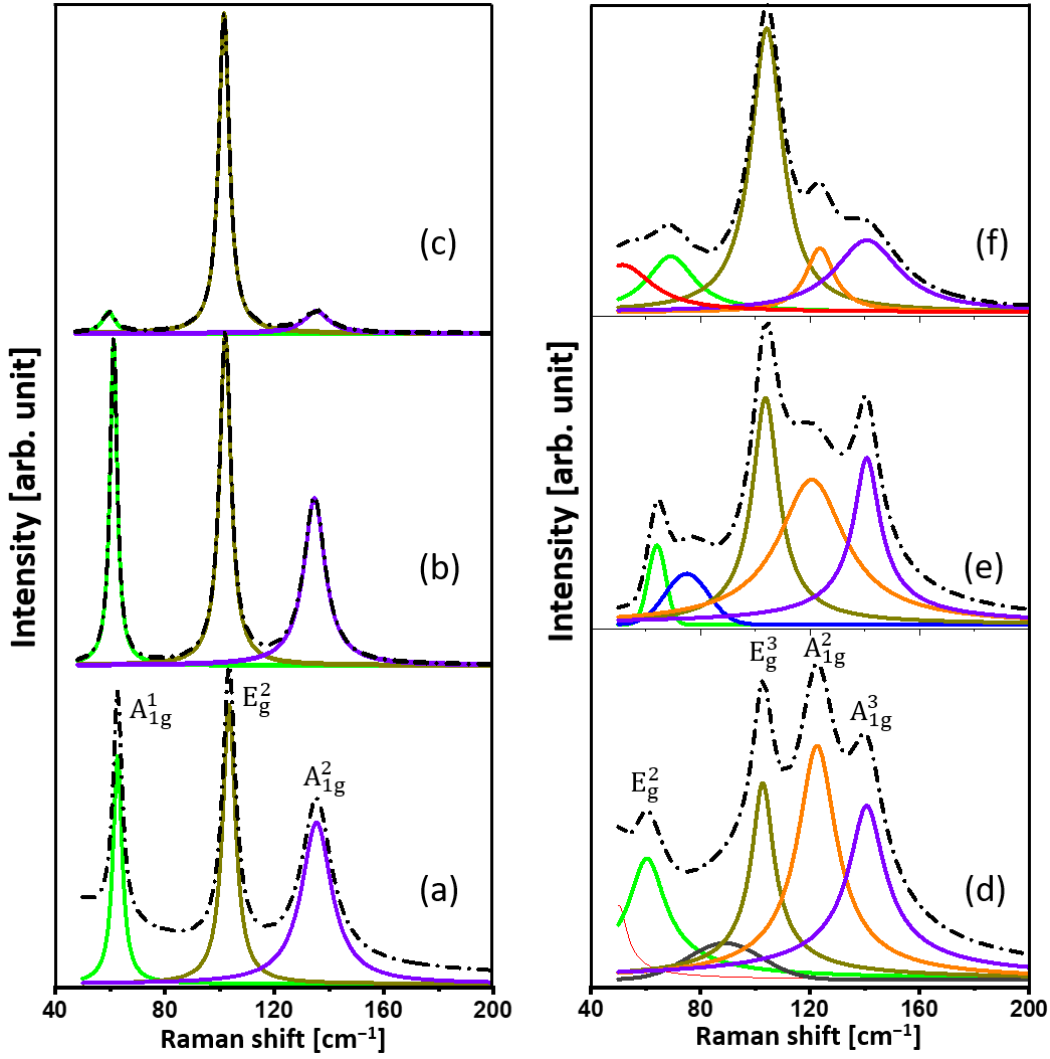
Fig. 6. Polarization-resolved Raman spectra of Bi_2Te_3 (a-c), and $MnBi_{1.7}Te_{2.8}$ (d-f); curves (a) and (d) H−H; curves (b) and (e) V−V; curves (c) and (f) V−H; excitation energy 2.3 eV.

The selection rule for the E_g phonons is the same as for dipole-allowed scattering. However, A_g mode corresponds to the Frohlich-interaction —induced (quadrupole-allowed) scattering [22, 23]. Hence, we expect to find E_g phonons in the V − H off-diagonal $z(x, y)\bar{z}$ scattering geometry and both A_g and E_g phonons in the H−H, and V−V diagonal $z(x, x)\bar{z}$ scattering configuration.

$$A_g = \begin{pmatrix} a & 0 & 0 \\ 0 & a & 0 \\ 0 & 0 & a \end{pmatrix}; E_g = \begin{pmatrix} c & 0 & 0 \\ 0 & -c & 0 \\ 0 & 0 & d \end{pmatrix}; E_g = \begin{pmatrix} 0 & -c & d \\ -c & a & 0 \\ d & 0 & 0 \end{pmatrix} \quad (5)$$

15

It means that E_g phonons in the $z(x, y)\bar{z}$ and A_g phonons in the $z(x, x)\bar{z}$ scattering configuration is expected. It is shown in the equation (5) that the off-diagonal elements of the A_g mode vanishes in the $V - H$ polarization geometry, on the other hand, E_g mode has non-vanishing off-diagonal elements in the matrix. However, both A_g and E_g modes has non vanishing diagonal elements in the matrix. The results clearly manifest that peak at 100 cm^{-1} in Bi$_2$Te$_3$ belong to E_g mode (E_g^2 symmetry) in $z(x, y)\bar{z}$ polarization direction. Two weak intensity peaks located left and right of the E_g^2 mode are A_{1g}^1 and A_{1g}^2 modes, respectively. The signature of these peaks in $z(x, y)\bar{z}$ polarization direction is associated to symmetry breaking of epitaxial direction. Peaks A_{1g}^1 and A_{1g}^2 modes along with E_g^3 mode are stronger in $H-H$ and $V-V$ scattering configuration which satisfies non zero diagonal matrix element allowed in $z(x, x)\bar{z}$ polarization direction.

In case of MBT film (MnBi$_{1.7}$Te$_{2.8}$), both Raman active E_g and A_{1g} modes are present in the $H-H$ and $V-V$ polarization direction. However, in $V - H$ polarization geometry, a strong E_g mode and weak intensity of all the A_{1g} modes was also observed. The excitation of A_{1g} modes indicate that the off-diagonal elements in the matrix is activated because the direction of crystal plane oriented off-diagonally. The intensity of the A_{1g}^2 is much stronger in the $H-H$ polarization direction in which the Bi atom is stationary and Te atoms below and above the central stationary Mn atom displaces antisymmetrically out-of-phase.

The intensity and peak shape of A_{1g}^2 mode is found to be sensitive to laser power as shown in Fig. 7.
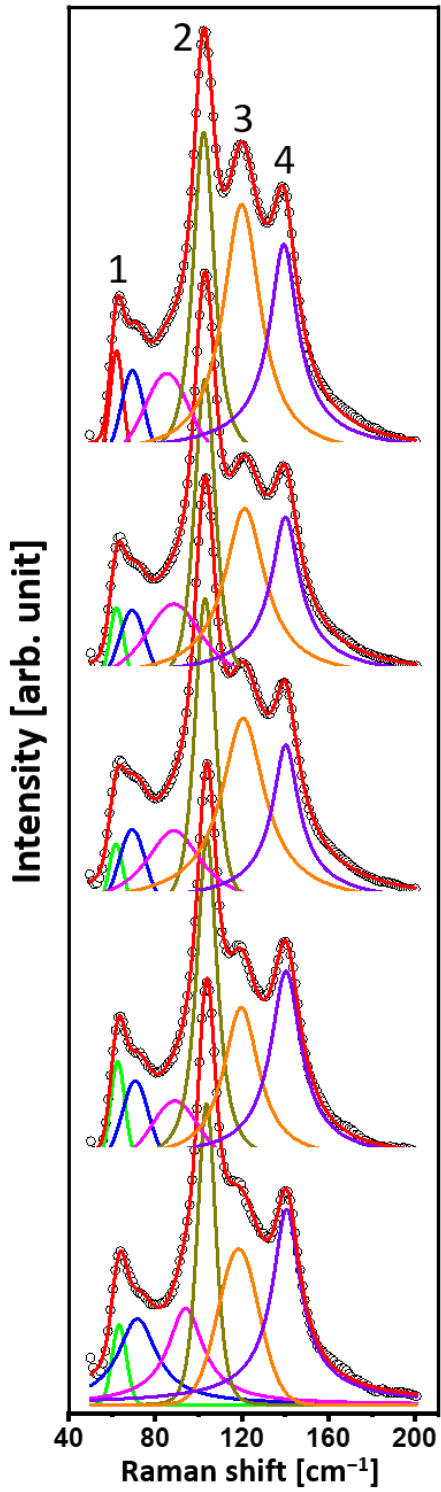
Fig. 7. Laser power dependent Raman spectra of MnBi$_{1.7}$Te$_{2.8}$ film (a) 0.05 mW (b) 0.1 mW (c) 0.25 mW (d) 0.5 mW (e) 1.0 mW; peaks 1, 2, 3 and 4 – E$_g^2$, E$_g^3$, A$_{1g}^2$ and A$_{1g}^3$.

The intensity of this mode increases and peak become more symmetric upon increase in laser power due to local heating which modify the lattice [29]. A peak shift and intensity variation

of other modes was not observed significantly which confirmed the absence of anharmoinc effect and thermal expansion of lattices due to heating.

4. Conclusions

Magnesium-based bismuth telluride and Bi_2Te_3 topological insulator thin films were grown by MBE method. Chemical composition dependent vibrational modes of these films was investigated by polarization-resolved Raman scattering spectroscopy with three different excitation energies 1.57, 1.94 and 2.33 eV. Intensity of vibrational modes was contrasting depending upon the elemental composition of magnesium-based bismuth telluride compounds. Intensity of E_g^3 TO mode was much stronger in Bi reach magnesium-based bismuth telluride compared to Bi deficient compound. However, intensity of A_{1g}^2 LO mode was stronger in Bi deficient magnesium-based bismuth telluride. E_g^3 TO mode corresponds to in-plane vibrations of Bi-Te atomic layers. The probability of vibrational cross section of this mode decreased due to deficiency of Bi atoms in the unit cell of magnesium-based bismuth telluride compound. Antisymmetric out-of-plane vibration of Te-Te atoms resulted in A_{1g}^2 LO mode, vibrational degree of freedom of this mode was stronger in Bi deficient compound. Intensity enhancement of E_g and A_{1g} mode was observed at lower excitation energy 1.57 eV associated to resonance effect.

Conflicts of interest

The authors declare no competing financial interest.

References

[1] L. Fu, C. L. Kane, Topological insulators with inversion symmetry, Phys. Rev. B 76 (2007) 045302− 045318.

[2] D. Hsieh, D. Qian, L. Wray, Y. Xia, Y. S. Hor, R. J. Cava, M. Z. Hasan, A topological Dirac insulator in a quantum spin Hall phase, Nature 452(2008) 970−975.

[3] H. Zhang, C. Liu, X. Qi, X. Dai, Z. Fang, S. Zhang, Topological insulators in Bi_2Se_3, Bi_2Te_3 and Sb_2Te_3 with a single Dirac cone on the surface, Nature Phys. 5 (2009) 438−442.

[4] Y. Xia, D. Qian, D. Hsieh, L. Wray, A. Pal, H. Lin, A. Bansil, D. Grauer, Y. S. Hor, R. J. Cava, Observation of a large-gap topological-insulator class with a single Dirac cone on the surface, Nature Phys. 5 (2009) 398−402.

[5] J. E. Moore, The birth of topological insulators, Nature 464 (2010) 194−198.

[6] D. Zhang, M. Shi, T. Zhu, D. Xing, H. Zhang, J. Wang, Topological axion states in the magnetic insulator $MnBi_2Te_4$ with the quantized magnetoelectric effect, Phys. Rev. Lett. 122 (2019) 206401−206406.

[7] C. Z. Chang, J. Zhang, X. Feng, J. Shen, Z. Zhang, M. Guo, K. Li, Y. Ou, P. Wei, L. L. Wang, Z. Q. Ji, Y. Feng, S. Ji, X. Chen, J. Jia, X. Dai, Z. Fang, S. C. Zhang, K. He, Y. Wang, L. Lu, X. C. Ma, Q. K. Xue, Experimental observation of the quantum anomalous Hall effect in a magnetic topological insulator, Science 340 (2013) 167–170.

[8] R. Yu, W. Zhang, H. J. Zhang, S. C. Zhang, X. Dai, Z. Fang, Quantized anomalous Hall effect in magnetic topological insulators, Science 329 (2010) 61–64.

[9] M. M. Otrokov, I. P. Rusinov, M. Blanco-Rey, M. Hoffmann, A. Yu. Vyazovskaya, S. V. Eremeev, A. Ernst, P. M. Echenique, A. Arnau, E. V. Chulkov, Unique thickness-dependent properties of the van der Waals interlayer antiferromagnet $MnBi_2Te_4$ films, Phys. Rev. Lett. 122 (2019) 107202− 107207.

[10] S. H. Lee, Y. Zhu, Y. Wang, L. Miao, T. Pillsbury, H. Yi, S. Kempinger, J. Hu, C. A. Heikes, P. Quarterman, W. Ratcliff, J. A. Borchers, H. Zhang, X. Ke, D. Graf, N. Alem, C. Z.

Chang, N. Samarth, Z. Mao, Spin scattering and noncollinear spin structure-induced intrinsic anomalous Hall effect in antiferromagnetic topological insulayor $MNBi_2Te_4$, Phys. Rev. Res. 1 (2019) 012011−012017.

[11] Y. L. Chen, J.-H. Chu, J. G. Analytis, Z. K. Liu, K. Igarashi, H.-H. Kuo, X. L. Qi, S. K. Mo, R. G. Moore, D. H. Lu, M. Hashimoto, T. Sasagawa, S. C. Zhang, I. R. Fisher, Z. Hussain, Z. X. Shen, Massive Dirac Fermion on the surface of a ьmagnetically doped topological insulator, Science 329 (2010) 659−662.

[12] S. Giraud, R. Egger, Electron-phonon scattering in topological insulators, Phys. Rev. B 83 (2011) 245322−245322.

[13] P. Mal, G. Bera, G. R. Turpu, S. K. Srivastava, A. Gangan, B. Chakraborty, B. Das, P. Das, Vibrational spectra of $Pb_2Bi_2Te_3$, $PbBi_2Te_4$ and $PbBi4Te_7$ topological insulators: Temperature dependent Raman and theoretical insight from DFT simulations, Phys. Chem. Chem. Phys. 21 (2019) 15030−15039

[14] A. A. Maksimov, I. I. Tartakovskii, Z. S. Aliev, I. R. Amiraslanov, N. A. Abdullaev, V. N. Zverev, Z. A. Jahangirli, I. Yu. Sklyadneva, M. M. Otrokov, N. T. Mamedov, E. V. Chulkov, Temperature Studies of Raman spectra in $MnBi_2Te_4$ and $MnSb_2Te_4$ magnetic topological insulators, JETP Lett. 2023, 118 (2023) 357–362.

[15] N. A. Abdullaev, I. R. Amiraslanov, Z. S. Aliev, Z. A. Jahangirli, I. Yu. Sklyadneva, E. G. Alizade, Y. N. Aliyeva, M. M. Otrokovd, V. N. Zverev, N. T. Mamedov, E. V. Chulkov, Lattice dynamics of Bi_2Te_3 and vibrational modes in Raman scattering of topological insulators $MnBi_2Te_4 \cdot n(Bi2Te3)$, JETP Lett. 115 (2022) 749–756.

[16] Y. Cho, J. Ho Kang, L. Liang, M. Taylor, X. Kong, S. Ghosh, F. Kargar, C. Hu, A. A. Balandin, A. A. Puretzky, N. Ni, C. W. Wong, Phonon modes and Raman signatures of $MnBi_{2n}Te_{3n+1}$ (n=1,2,3,4) magnetic topological heterostructures, Phys. Rev. Res. 4 (2022) 013108−013114.

[17] T. Beechem, S. Graham, Temperature and doping dependence of phonon lifetimes and decay pathways in GaN, J. Appl. Phys. 103 (2008) 093507−093507.

[18] A. Chernikov, V. Bornwasser, M. Koch, S. Chatterjee, C. N. Bottge, T. Feldtmann, M. Kira, S. W. Koch, Phonon-assisted luminescence of polar semiconductors: Frohlich coupling versus ¨ deformation-potential scattering, Phys. Rev. B 85 (2012) 035201−035208.

[19] J.A. Sobota, S.-L. Yang, A.F. Kemper, J.J. Lee, F.T. Schmitt, W. Li, R.G. Moore, J.G. Analytis, I.R. Fisher, P.S. Kirchmann, T.P. Devereaux, Z.-X. Shen, Direct optical coupling to an unoccupied Dirac surface state in the topological insulator Bi_2Se_3, Phys. Rev. Lett. 111 (2013) 135802−135806.

[20] D. Niesner, Th. Fauster, S.V. Eremeev, T.V. Menshchikova, Yu. M. Koroteev, A. P. Protogenov, E.V. Chulkov, O.E. Tereshchenko, K.A. Kokh, O. Alekperov, A. Nadjafov, N. Mamedov, Unoccupied topological states on bismuth chalcogenides, Phys. Rev. B 86 (2012) 205403−205403.

[21] 41. H. Soifer, A. Gauthier, A. F. Kemper, C. R. Rotundu, S. L. Yang, H. Xiong, D. Lu, M. Hashimoto, P. S. Kirchmann, J. A. Sobota and Z. X. Shen, Band-resolved imaging of photocurrent in a topological insulator, Phys. Rev. Lett., 2019, **122**, 167401–167407.

[22] J. Menendez, M. Cardona, Interference effects: A key to understanding forbidden Raman scattering by LO phonons in GaAs, Phys. Rev. B 31 (1985) 3696−3704.

[23] W. Hayes and R. Loudon, Scattertng of Light by Crystals (Wiley, New York, 1978).

[24] A. C. Lee, H.-H. Kung, Xueyun Wang, S.-W. Cheong, G. Blumberg, Electronic and vibrational excitations on the surface of the three-dimensional topological insulator $Bi_2Te_{3-x}Se_x$(x=0,2,3), Phys. Rev. B 108 (2023) 174301.

[25] Hao Xu, Yuxin Song, Qian Gong, Wenwu Pan, Xiaoyan Wu, Shumin Wang, Raman spectroscopy of epitaxial topological insulator Bi_2Te_3 thin films on GaN substrates, Mod. Phys. Lett. B 29 (2015) 1550075−1550084.

[26] I. Boulares, G. Shi, E. Kioupakis, P. Lostak, C. Uher, R. Merlin, Surface phonons in the topological insulators Bi_2Se_3 and Bi_2Te, Solid State Commun. 271 (2018) 1−5.

[27] R. German, E.V. Komleva, P. Stein, V.G. Mazurenko, Z. Wang, S.V. Streltsov, Y. Ando, P.H.M. van Loosdrecht, Phonon mode calculations and Raman spectroscopy of the bulk-insulating topological insulator $BiSbTeSe_2$, Phys. Rev. Mater. 3 (2019) 054204− 054209.

[28] A. K. Sood, J. Menendez, M. Cardona, K. Ploog, Resonance Raman scattering by confined LO and TO phonons in GaAs-A1As superlattices, Phys. Rev. Lett. 54 (1985) 2111−2114.

[29] Xinliang Chen, Honglai Li, Zhaoyang Qi, Tiefeng Yang, Yankun Yang, Xuelu Hu, Xuehong Zhang, Xiaoli Zhu, Xiujuan Zhuang, Wei Hu, Anlian Pan, Synthesis and optoelectronic properties of quaternary GaInAsSb alloy nanosheets, Nanotechnology 27 (2016) 505602−505610.